

A STUDY OF X-RAY POINT SOURCES IN HEILES CLOUDS 1 AND 2

NÓRA VARGA^{a,*}, ANDRÁS PÉTER JOÓ^a, BENDEGÚZ KONCZ^{a,b}

^a Eötvös Loránd University, Department of Astronomy, Pázmány Péter sétány 1/A, 1117 Budapest, Hungary

^b Doctoral School of Physics at University of Debrecen, Bem tér 18/B, 4026 Debrecen, Hungary

* corresponding author: varganora43@gmail.com

ABSTRACT. Star formation takes place in the coldest parts of molecular clouds, beginning in the densest, collapsing regions of filaments. As pre-main sequence stars are luminous X-ray emitters, X-ray point sources can serve as effective tracers of YSOs. In our study, we examined the distribution of X-ray point sources in two nearby molecular clouds: Heiles Cloud 2 (HCL 2), a ring-like molecular cloud complex in the Taurus region, and Heiles Cloud 1 (LDN 1251), a cometary-shaped dark molecular cloud. By incorporating the latest YSO catalogue from Gaia DR3, we analysed how YSO positions compare to the structure of the interstellar medium (ISM) and found that the sources are primarily aligned just outside the densest regions. Additionally, we compared the positions with the magnetic field structure and found no clear correlation at the given resolution.

KEYWORDS: ISM, YSO, polarisation, magnetic field.

1. INTRODUCTION

Star formation takes place in the coldest, densest parts of the interstellar medium (ISM), in the molecular clouds. The term “cloud” is used to refer to structures in the interstellar medium that are separated from their surroundings by a sharp change in some physical or chemical property. The ISM is highly filamentary, and these filaments have been recognized as important environments for star formation and the growth of new stars in these dense, active regions [1]. In wavelength ranges where strong, diffuse galactic background radiation dominates, such as in the far-infrared range, we can use the absorption of dust against the continuum radiation to study the structure of clouds. Examples of this methodology are the works of Bacmann et al. [2] and Stutz et al. [3], which demonstrated that detailed images of the internal structure of clouds and cores can be obtained using this technique. The Herschel Space Telescope has mapped the sky at far-infrared and submillimetre wavelengths providing data on the highly structured ISM [4].

Molecular clouds have high density cores, which are the densest regions where gravity pulls the gas together. Star formation begins with the gravitational collapse of dense, rotating, magnetic molecular cloud cores. Due to angular momentum conservation, this process is always accompanied by the formation of circumstellar disks (e.g. Shu, Adams & Lizano 1987), sometimes still embedded in their envelope. The evolution of young stars in the first few million years after they emerge from their protostellar dusty envelopes is characterised by the presence of circumstellar disks and intense magnetic fields. Pre-main sequence stars are luminous X-ray sources due to the accretion process. Young stars emit X-rays with a luminosity sev-

eral orders of magnitude higher than that of older field stars (Preibisch & Feigelson 2005 [5]). As a result, X-ray observations have proven to be a highly effective method for identifying stellar members of young star-forming complexes, even in highly contaminated fields. This approach is relatively unbiased by the presence or absence of circumstellar disks (e.g., [6, 7]). These observations of star-forming regions allow for the study of high-energy processes in YSOs, which are of great importance for our understanding of the star formation process. However there are a number of other types of X-ray point sources, including extragalactic ones. In our pilot study, we are attempting a comparative study of the distribution of X-ray point sources, the cold interstellar medium, and the pattern of the dust linear polarisation in the Heiles Cloud 1 and Heiles Cloud 2 (see [8]).

Heiles Cloud 1 is better known as LDN 1251 [9]. It is an elongated molecular cloud at the boundary of the Cepheus Flare giant molecular cloud (see [10, 11]). It contains dense cores (see e.g. [12]) and a number of young stellar objects (see e.g. [13, 14]) with two of those, IRAS22343+7501 and IRAS22376+7455, showing water maser emission (see [15] and [16], respectively). The cloud is elongated, which could be the result of a low-velocity shock encounter according to [17], while [18] also investigated processes related to the magnetic field. The distance of LDN 1251 is around 340–350 pc [19–21].

Heiles Cloud 2 (HCL 2) is a large cloud in the Taurus Molecular Cloud complex. HCL 2 is sometimes referred to as TMC-1, although the TMC-1 ridge is only part of it (see e.g. [22]). HCL 2 is active in star formation with all phases present: starless cores (see e.g. [22]) protostars (see e.g. [23, 24]) and more evolved YSOs (see e.g. [22]). We will focus on the

TMC-1 in our study. The distance of HCL 2 is around 140 pc [21].

Recently, [25] compared the pattern of polarisation seen in images created from Planck polarisation data to that of the distribution of a cold ISM. LDN1251 and HCL-2 showed quite different relations.

2. DATA AND METHODS

2.1. HEILES CLOUD 2

To examine the structure of the HCL 2, we use the infrared data from the Herschel SPIRE at 500 μm centered on RA(J2000) = 4 h 41 m Dec(J2000) = 25°46'. We can see, in Figure 1, where the molecular cloud is shown in the galactic coordinate system, that the molecular cloud has a ring-like structure and it identifies as the most massive molecular cloud complex in the Taurus region. HCL 2 is divided into four main clouds:

- (1.) TMC-1,
- (2.) HCL2-A,
- (3.) HCL2-B, and
- (4.) HCL2-E, HCL2-ES.

The research primarily focused on the narrow, fragmented ridge located in the eastern part of the HCL 2, referred to as Taurus Molecular Cloud 1 (TMC-1) [22].

2.2. TAURUS MOLECULAR CLOUD 1 (TMC1)

Because of X-ray data availability, we focused on the TMC1 part of the HCL 2 and examined the distribution of X-ray point sources from the XMM-OM Serendipitous Source Survey Catalog X-ray data [26]. To further confirm and to find additional X-ray observations, we add XMM-Newton Extended Survey of Taurus Molecular Cloud [27]. For the position of YSOs, we used Gaia DR3 data because it contains sources with reliable astrometry and analysis of their proper motions. Then, we cross-correlated these with a YSO sample by Gábor Marton (in prep.).

2.3. MATCHING SOURCES IN HCL 2

After cross-matching the X-ray data and the location of YSOs, we found three matching sources (see Figure 2). The observation of YSOs is not straightforward, since they show a wide range of physical properties. The evolution of YSOs in the first few million years, after they emerge from their protostellar dusty envelopes, is characterised by the presence of circumstellar disks. For the classification of the YSOs, we examine their spectral energy distribution (SED), because as a YSO ages, its circumstellar environment changes, and this change is reflected in the shape of its SED. For the determination of the state of the star formation, we look at the infrared excess that comes from the dust in the ISM surrounding the object and is superimposed on the YSO's black body radiation. Class I objects are protostars that accrete material on their forming discs and have regular outflows at

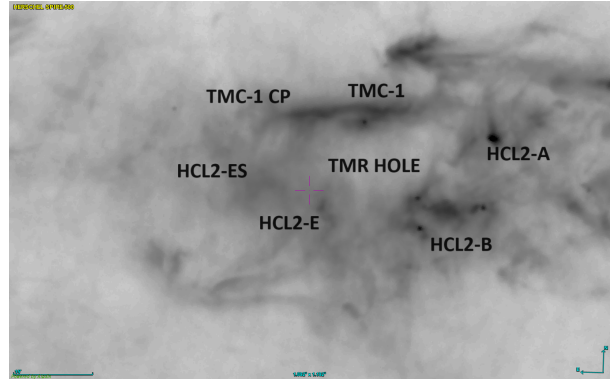


FIGURE 1. The four main clouds in the HCL 2 on the Herschel 500 μm infrared image.

their poles. Class II objects are still embedded but with a thinner disc with less infrared excess. Class III objects are pre-main sequence stars with only a faint disk.

In Figure 2, we can see the three matching sources in the HCL 2. We examined their classification based on their SED and found that:

- (1.) is Haro 6-33 (see Figure 3), a T Tauri star at the TMC-1C. It is a class I object, where we observe a rising spectrum up to around 3 μm , followed by a flat spectrum between 3 and 22 μm caused by the presence of a substantial, infalling, circumstellar envelope [28].
- (2.) is JH 223 TT* (see Figure 4), a class II YSO at TMC-1. Its SED is characterised by a decreasing flux in the 3–22 μm wavelength range. For this type of object, the emission comes only from an optically thick circumstellar disk [28].
- (3.) is XEST 07-024 (see Figure 5), a class III YSO in the TMR Hole, with only a small infrared excess.

The spectral energy distributions in Figures 3, 4, and 5 are derived from the photometric data taken from VizieR. The different colours indicate different sources for the data, as detailed in the appendix Table 3. The error bars represent the uncertainties of the respective measurements. Since the data points are collected from different surveys (as indicated by the colours), the presence and magnitude of the error bars depend on the original data sources.

2.4. HEILES CLOUD 1

The cometary-shaped LDN 1251 is one of the prominent molecular clouds of the Cepheus region. We study the cloud in the 500- μm infrared with Herschel. For the position of YSOs, we use cross-correlated Gaia DR3 data with a YSO sample by Gábor Marton (in prep.). For the X-ray data, we use the XMM-Newton Serendipitous Source Catalogue 4XMM-DR13 [29] and MORX (Millions of Optical-Radio/X-ray Associations) catalogue [30], which contains the LASS, LoTSS, RACS, FIRST, NVSS, and SUMSS radio sur-

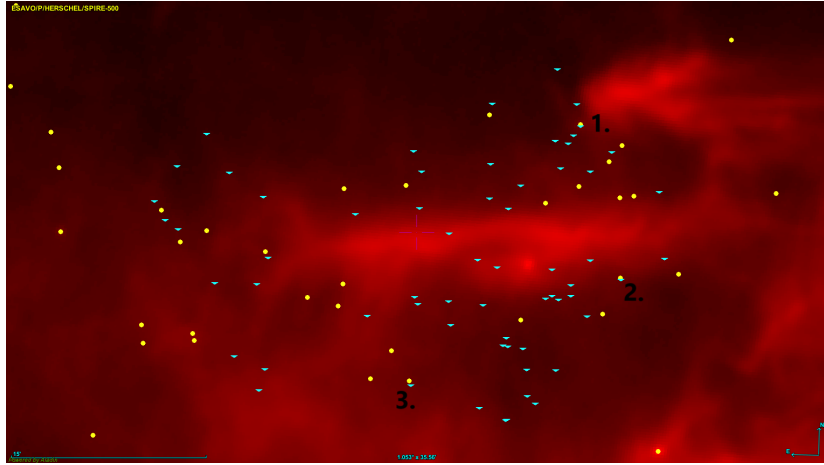


FIGURE 2. Herschel 500 μm image of the Heiles Cloud 2 with the TMC-1 ridge in the centre, the TMR Hole below it, and the TMC-1C in the upper right corner. We overlaid X-ray point sources (blue triangles) and YSOs (yellow circles), and marked the positions of three selected YSOs (see text).

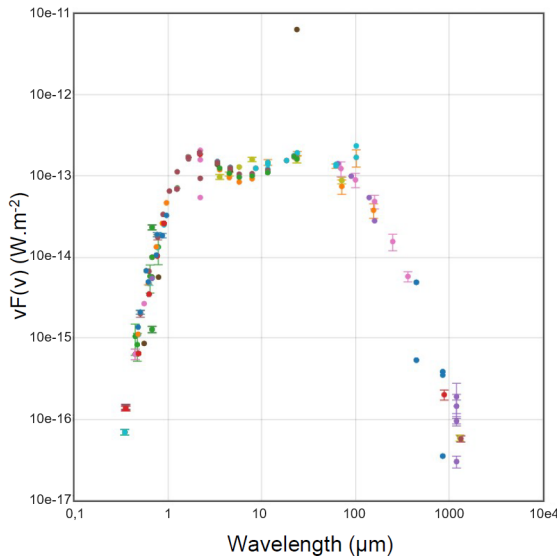


FIGURE 3. SED of Haro 6-33, a class I YSO in HCL 2. Description of the data points in Table 3.

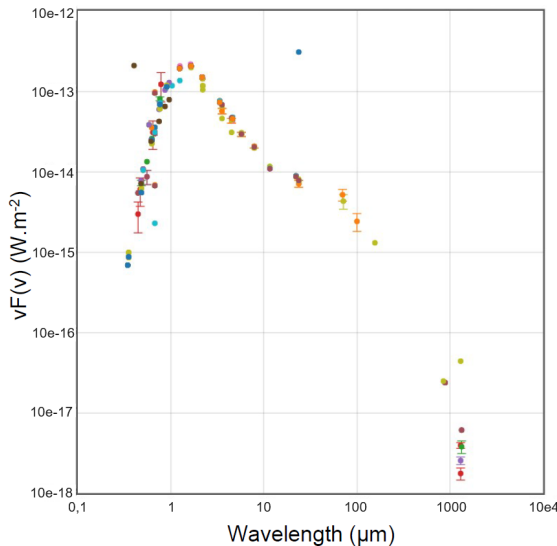


FIGURE 4. SED of JH 223, a class II YSO in HCL 2. Description of the data points in Table 4.

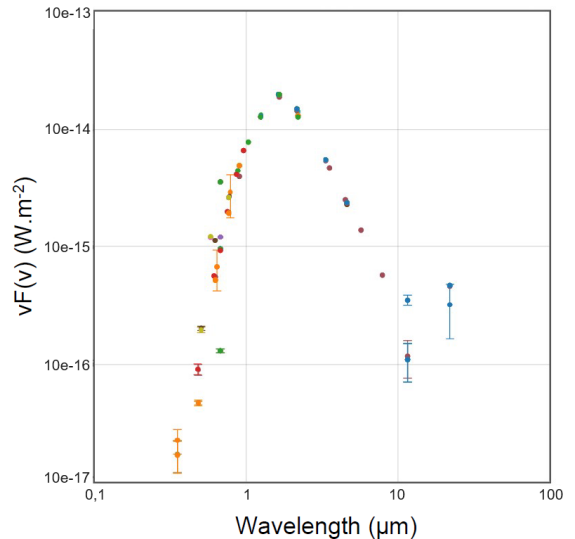


FIGURE 5. SED of XEST 07-024, a class III YSO in HCL 2. Description of the data points in Table 5.

veys, and Chandra, XMM-Newton, Swift, and ROSAT X-ray surveys.

2.5. HARDNESS RATIO

The hardness of X-ray point sources can be determined by calculating the hardness ratio and it is used to show spectral properties. The purpose of investigating the X-ray point sources is to draw conclusion of YSO candidates using the hardness ratio (see in Hardness ratio) of each X-ray source. With the help of this index, we can compare the position of the YSO candidates and the YSOs from the Gaia DR3. Some spectral information on faint sources can be derived from the X-ray hardness ratio, defined as:

$$\text{HR} = \frac{H - S}{H + S}$$

where S and H are the number of counts in the soft and hard bands, respectively. The HR values

RA (J2000)	DE (J2000)	HR
04 40 39.13	+25 40 04.3	-0.206
04 40 49.54	+25 51 20.0	-0.811
04 40 47.15	+25 47 31.6	0.043
04 41 04.32	+25 57 55.5	-0.837
04 41 24.70	+25 54 48.4	-0.306
04 41 25.91	+25 43 47.7	-0.203
04 41 29.67	+25 38 14.5	-0.264
04 41 58.91	+25 57 50.4	-0.389
04 42 11.83	+25 31 27.3	-0.334
04 41 36.12	+25 49 59.5	0.005
04 41 38.80	+25 56 27.4	-0.105
04 40 37.41	+25 37 41.1	-0.137
04 42 28.97	+25 34 09.7	-0.18
04 40 39.75	+25 43 01.7	0.094
04 41 27.12	+25 38 04.8	-0.063
04 41 37.83	+25 55 35.9	-0.074
04 41 40.42	+25 54 12.9	0.081
04 42 04.45	+25 38 45.8	-0.06
04 42 07.41	+25 29 29.6	-0.012
04 42 08.51	+25 45 19.5	0.086
04 41 38.95	+25 24 26.5	-0.022
04 41 07.33	+25 33 41.5	0.071
04 42 08.51	+25 45 19.5	0.057

TABLE 1. The coordinates and hardness ratio of YSO candidates found in HCL 2.

can be compared to that of the YSO in the EDR in order to select new YSO candidates. Negative values indicate a soft spectrum and positive values indicate a hard spectrum [31]. After applying this formula to the X-ray sources and determining the hardness ratio, we used the 0.5–1.0 keV and 1.0–2.0 keV bands. To define the YSO candidates, we followed the criteria from a previous publication [32], considering sources with hardness ratio values in the range of -1.0 to 0.1 as potential YSOs. As a result, we identified 20 YSO candidates in HCL 2, as shown in Table 1. The HR values for the three matching sources are as follows: Haro 6-33 has an HR value of -0.105, JH 223 has -0.811, and XEST 07-024 has 0.071.

Table 2 shows the 30 YSO candidates in LDN 1251 based on their HR values.

We used the XMM-Newton survey HR data [33] for the point sources we examined.

3. RESULTS

We cross-matched the X-ray sources with YSOs in TMC-1 and LDN 1251, and investigated which of the X-ray sources could be YSO candidates to compare them with known YSOs from Gaia. However, the YSO candidates identified in these two clouds do not necessarily correspond to the matched sources, indicating that some potential young stellar objects may not yet be confirmed or classified as known YSOs.

In TMC-1, we identified 63 X-ray point sources, three of which matched known YSOs. As shown in Figure 2, the distribution of X-ray sources (blue rhombs) and YSOs (yellow circles) reveals that they tend to be located around, rather than within, the densest parts of the cloud. This suggests that while ongoing star formation occurs in the densest regions, aligned

RA (J2000)	DE (J2000)	HR
342.957757	+75.096472	-0.653135
339.666273	+75.238812	-0.628847
343.785354	+75.004985	-0.585712
343.140114	+75.217713	-0.530832
339.781313	+75.175109	-0.529483
343.137091	+75.229216	-0.523715
339.443125	+75.143217	-0.513268
339.031998	+75.359255	-0.464459
338.657758	+75.192675	-0.431929
342.488747	+75.104120	-0.426178
343.166193	+75.071182	-0.384939
343.451572	+75.106704	-0.378140
343.590204	+74.965667	-0.314152
343.285043	+75.053685	-0.309921
342.738687	+75.108034	-0.303983
339.645200	+75.200929	-0.288714
342.420129	+75.025788	-0.283266
339.677343	+75.196029	-0.280326
342.525642	+75.128734	-0.262991
339.619931	+75.249014	-0.248900
343.009320	+75.164331	-0.227124
343.285296	+75.039826	-0.216046
339.050367	+75.212686	-0.194606
343.793039	+74.954663	-0.192297
339.829930	+75.197401	-0.165193
342.484131	+75.043194	-0.160678
339.887683	+75.221501	-0.130436
342.473185	+75.120343	-0.126321
342.430687	+75.190120	-0.100328
342.560594	+74.920663	-0.097193
339.863918	+75.174516	-0.094893
339.400663	+75.097643	-0.073893
343.317712	+75.071321	-0.060079
339.550711	+75.204772	-0.025209
339.594040	+75.192727	-0.011237
339.867444	+75.399739	0.024469
339.811320	+75.121159	0.046853
343.104486	+74.890597	0.083169
340.096978	+75.204793	0.085564
343.956811	+75.123575	0.088863
338.674788	+75.238829	0.093959
343.236888	+75.158129	0.129253
343.058150	+75.055343	0.144405
339.022812	+75.308814	0.227217
342.475152	+75.167733	0.238902
343.408966	+75.289887	0.240431
343.165062	+75.105772	0.262984
339.434881	+75.223244	0.265742
339.965553	+75.326335	0.272838
338.640705	+75.286671	0.284856
343.721962	+75.128206	0.287354
343.679722	+75.045595	0.312120
342.592285	+75.157863	0.314148
339.578423	+75.198197	0.339752
339.365938	+75.257064	0.344141
339.439293	+75.346271	0.359463
338.819306	+75.313116	0.372662
338.858168	+75.175652	0.380989
342.778512	+75.130965	0.413904
339.929106	+75.240813	0.417928
342.630871	+75.095338	0.421081
343.247715	+75.163632	0.432724
340.226454	+75.156715	0.437377
339.917555	+75.222679	0.437697
339.725959	+75.321172	0.439713
343.775427	+75.201870	0.451005
343.527466	+75.078175	0.477650
342.293686	+75.011957	0.485013
339.375895	+75.134971	0.496110
343.924093	+75.162493	0.503376

TABLE 2. The coordinates and hardness ratios of YSO candidates found in LDN 1251.

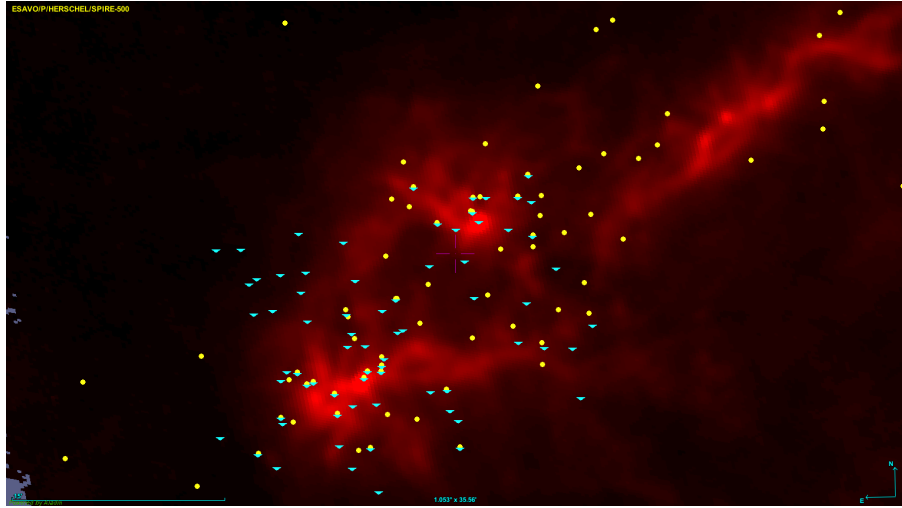


FIGURE 6. Herschel 500- μ m image of LDN 1251 with the X-ray sources (blue triangles) and YSOs (yellow circles).

with the structure of the cloud, young stars and X-ray sources become more detectable as they emerge from their birth sites, where extinction is lower.

Similarly, in LDN 1251, we found 64 X-ray point sources, 20 of which matched known YSOs. Figure 6 illustrates that both X-ray sources and YSOs are positioned around the cloud rather than deeply embedded in the most opaque regions. This spatial distribution is consistent with the expectation that young stellar objects, especially those in later evolutionary stages, become more visible in X-rays once they have cleared away some of their surrounding material. Additionally, the correlation between the X-ray sources and the YSOs outside the densest areas may indicate regions of recent or ongoing star formation, where emerging stars become X-ray active as they evolve.

3.1. POLARISATION

The phenomenon of polarisation was described as early as the 1950s [34], and since then, it has remained one of the most important methods for studying the structure of magnetic fields. Magnetic fields play a crucial role in star formation processes at all scales. A precise and detailed determination of their properties – including strength and spatial orientation – is essential for a thorough understanding of the physical characteristics of molecular clouds, star cores, and protoplanetary disks. For the investigation of the magnetic field associated with star-forming regions, we examined the polarised dust emission. This method, which involves studying polarised emission in the far-infrared and millimeter wavelength ranges, is one of the most suitable techniques for exploring the magnetic field of molecular clouds [35].

Using Planck's all-sky intensity and polarisation maps at 353 GHz, we extracted the regions HCL 1 and HCL 2 and calculated the magnetic field orientation. We used a Line Integral Convolution (LIC) method to visualise the field lines and blended these with the intensity maps, imprinting the field structure

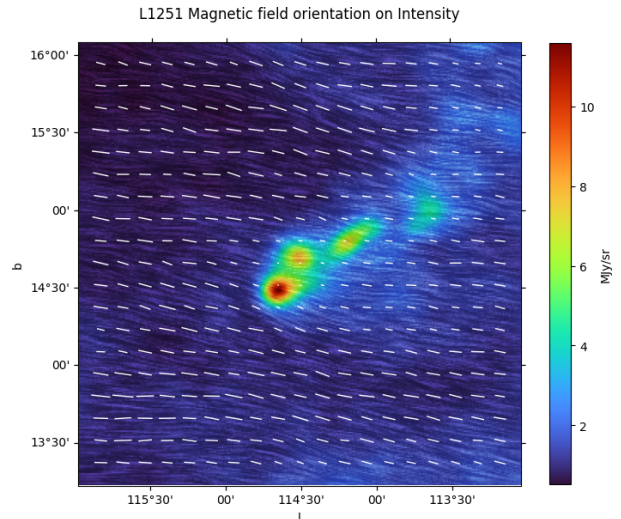


FIGURE 7. Magnetic field orientation and relative strength perpendicular to the line of sight in LDN 1251 based on Planck polarimetry data. The field structure is visualised using an LIC method blended with intensity, with an overlaid vector field representation indicating the relative field strength perpendicular to the line of sight.

as darker lines. This allowed us to observe the relationship between the intensity and the magnetic field orientation.

In Figures 7 and 8, we also overlaid a vector representation of the magnetic field onto the LIC composite to observe the relative field strength in different areas of LDN 1251 and HCL 2. The vectors' length shows the intensity of the magnetic field's transverse component to the line of sight. Because of this, a shorter vector can also mean a rotation of the magnetic field. Figures 9 and 10 show YSOs as white plus (+) and X-ray point sources as yellow cross (x) symbols, overlaid on the LIC composite of the intensity and magnetic field. The majority of the YSOs are concentrated in the dense part of the clouds.

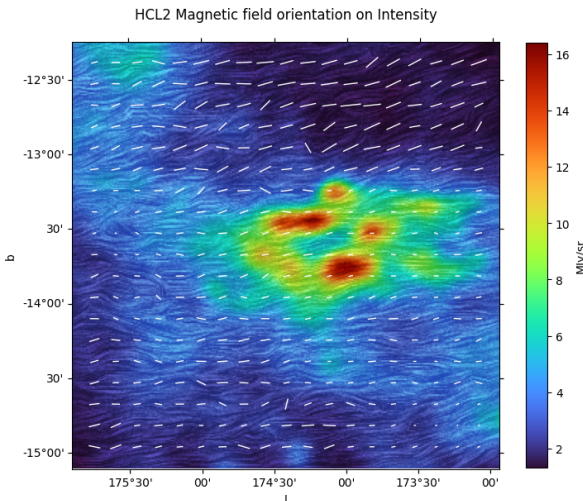


FIGURE 8. Magnetic field orientation and relative strength perpendicular to the line of sight in HCL 2 based on Planck polarimetry data. The field structure is visualised using an LIC method blended with intensity, with an overlaid vector field representation indicating the relative field strength perpendicular to the line of sight.

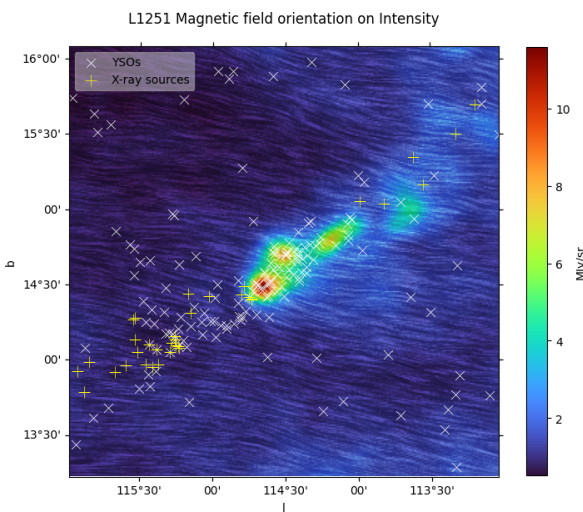


FIGURE 9. Magnetic field orientation in LDN 1251 based on Planck polarimetry data, with overlaid YSOs as plus (+) and X-ray point sources as cross (x) symbols. The field structure is visualised using an LIC method blended with intensity.

3.2. COMPARISON

The vectors indicate the direction of the magnetic field. Both cloud's magnetic field vectors are aligned, suggesting a more ordered magnetic field. But we could not make any assumptions about the structure of the magnetic field, for that we need a higher resolution. In the future, we plan to conduct a correlation analysis to examine the relationship between the magnetic field properties and other characteristics of the clouds. A more detailed and in-depth investigation of the magnetic field will be carried out later, including comparative studies to better understand its role in the cloud dynamics.

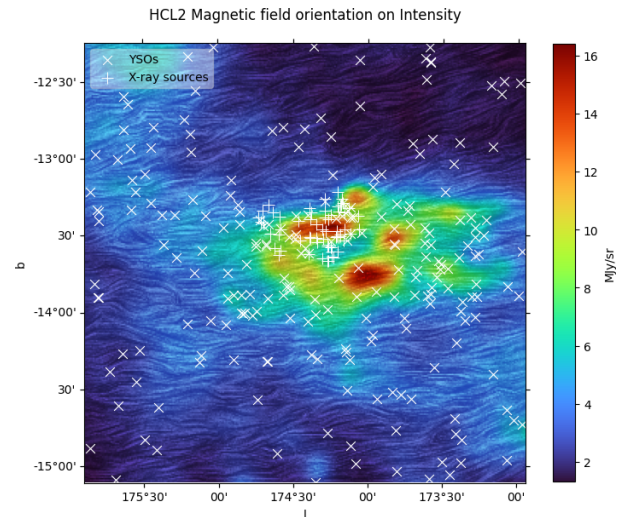


FIGURE 10. Magnetic field orientation in HCL 2 based on Planck polarimetry data, with overlaid YSOs marked as plus (+) and X-ray point sources as cross (x) symbols. The field structure is visualised using an LIC method blended with intensity.

ACKNOWLEDGEMENTS

The IBWS conference participation of B. Koncz was subsidized by the Dean's Council of ELTE Eötvös Loránd University Faculty of Science, Budapest.

This research has made use of the SIMBAD database, operated at CDS, Strasbourg, France [36].

This research has made use of Aladin sky atlas developed at CDS, Strasbourg Observatory, France [37].

This research has made use of the VizieR catalogue access tool, CDS, Strasbourg, France. The original description of the VizieR service was published in [38].

We are grateful to L. Viktor Tóth for his supervision of this work.

REFERENCES

- [1] R. C. Kennicutt, N. J. Evans. Star formation in the Milky Way and nearby galaxies. *Annual Review of Astronomy & Astrophysics* **50**:531–608, 2012. <https://doi.org/10.1146/annurev-astro-081811-125610>
- [2] A. Bacmann, P. Andre, J.-L. Puget, et al. An ISOCAM absorption survey of the structure of pre-stellar cloud cores. *Astronomy & Astrophysics* **361**:555–580, 2000. <https://doi.org/10.48550/arXiv.astro-ph/0006385>
- [3] A. M. Stutz, J. H. Bieging, G. H. Rieke, et al. Spitzer observations of a 24 μm shadow: Bok globule CB 190. *The Astrophysical Journal* **665**(1):466, 2007. <https://doi.org/10.1086/519488>
- [4] P. André, A. Men'shchikov, S. Bontemps, et al. From filamentary clouds to prestellar cores to the stellar IMF: Initial highlights from the Herschel Gould belt survey. *Astronomy & Astrophysics* **518**:L102, 2010. <https://doi.org/10.1051/0004-6361/201014666>
- [5] T. Preibisch, E. D. Feigelson. The evolution of X-ray emission in young stars. *The Astrophysical Journal Supplement Series* **160**(2):390, 2005. <https://doi.org/10.1086/432094>

- [6] E. D. Feigelson, L. K. Townsley, P. S. Broos, et al. Overview of the Massive Young Star-forming Complex study in Infrared and X-Ray (MYStIX) project. *The Astrophysical Journal Supplement Series* **209**(2):26, 2013. <https://doi.org/10.1088/0067-0049/209/2/26>
- [7] L. K. Townsley, P. S. Broos, G. P. Garmire, et al. The massive star-forming regions omnibus X-ray catalog. *The Astrophysical Journal Supplement Series* **213**(1):1, 2014. <https://doi.org/10.1088/0067-0049/213/1/1>
- [8] C. E. Heiles. Normal OH emission and interstellar dust clouds. *The Astrophysical Journal* **151**:919, 1968. <https://doi.org/10.1086/149493>
- [9] B. T. Lynds. Catalogue of dark nebulae. *The Astrophysical Journal Supplement Series* **7**:1, 1962. <https://doi.org/10.1086/190072>
- [10] Z. T. Kiss, L. V. Tóth, O. Krause, et al. Star formation in the Cepheus Flare region: Implications from morphology and infrared properties of optically selected clouds. *Astronomy & Astrophysics* **453**(3):923–936, 2006. <https://doi.org/10.1051/0004-6361:20053235>
- [11] M. Szilágyi, M. Kun, P. Ábrahám. The Gaia view of the Cepheus Flare. *Monthly Notices of the Royal Astronomical Society* **505**(4):5164–5182, 2021. <https://doi.org/10.1093/mnras/stab1496>
- [12] L. V. Toth, C. M. Walmsley. Star formation in L 1251. II. “The next generation” – NH₃ cores. *Astronomy & Astrophysics* **311**:981–988, 1996.
- [13] L. Pasztor, L. V. Toth, L. G. Balazs. Searching for embedded clusters in the Cepheus-Cassiopeia region. *Astronomy & Astrophysics* **268**:108–115, 1993.
- [14] M. Kun, T. Prusti. Star formation in L 1251: Distance and members. *Astronomy & Astrophysics* **272**:235–242, 1993.
- [15] V. L. Toth, C. M. Walmsley. Water masers in L1251. *Information Bulletin on Variable Stars* **4107**:1, 1994.
- [16] L. V. Toth, M. Kun. New water maser in L1251. *Information Bulletin on Variable Stars* **4492**:1, 1997.
- [17] L. V. Tóth, A. Horváth, L. K. Haikala. Low velocity shock-cloud encounters II. Observations and interpretation. *Astrophysics and Space Science* **233**(1):175–179, 1995. <https://doi.org/10.1007/BF00627347>
- [18] E. Sharma, G. Maheswar, S. Dib. Cloud motion and magnetic fields: Four clouds in the Cepheus Flare region. *Astronomy & Astrophysics* **658**:A55, 2022. [Erratum: *Astronomy & Astrophysics* **659**:C2, 2022]. <https://doi.org/10.1051/0004-6361/202140495>
- [19] L. G. Balázs, P. Ábrahám, M. Kun, et al. Star count analysis of the interstellar matter in the region of L1251. *Astronomy & Astrophysics* **425**(1):133–141, 2004. <https://doi.org/10.1051/0004-6361:20047059>
- [20] C. Zucker, J. S. Speagle, E. F. Schlafly, et al. A compendium of distances to molecular clouds in the Star formation handbook. *Astronomy & Astrophysics* **633**:A51, 2020. <https://doi.org/10.1051/0004-6361/201936145>
- [21] M. Zhang. Distances to nearby molecular clouds traced by young stars. *The Astrophysical Journal Supplement Series* **265**(2):59, 2023. <https://doi.org/10.3847/1538-4365/acc1e8>
- [22] L. V. Tóth, M. Haas, D. Lemke, et al. Very cold cores in the Taurus molecular ring as seen by ISO. *Astronomy & Astrophysics* **420**(2):533–546, 2004. <https://doi.org/10.1051/0004-6361:20035611>
- [23] D. Apai, L. V. Tóth, T. Henning, et al. HST/NICMOS observations of a proto-brown dwarf candidate. *Astronomy & Astrophysics* **433**(2):L33–L36, 2005. <https://doi.org/10.1051/0004-6361:200500098>
- [24] Ł. Tychoniec, M. L. van Gelder, E. F. van Dishoeck, et al. JWST Observations of Young protoStars (JOYS). Linked accretion and ejection in a class I protobinary system. *Astronomy & Astrophysics* **687**:A36, 2024. <https://doi.org/10.1051/0004-6361/202348889>
- [25] L. V. Tóth, O. Fehér, M. Juvela, et al. HCL1 and HCL2 – low mass star formation in violent and quiet environments. *Proceedings of the International Astronomical Union* **14**(S345):333–334, 2018. <https://doi.org/10.1017/S1743921319001741>
- [26] M. J. Page, C. Brindle, A. Talavera, et al. The XMM-Newton serendipitous ultraviolet source survey catalogue. *Monthly Notices of the Royal Astronomical Society* **426**(2):903–926, 2012. <https://doi.org/10.1111/j.1365-2966.2012.21706.x>
- [27] M. Güdel, K. R. Briggs, K. Arzner, et al. The XMM-Newton extended survey of the Taurus molecular cloud (XEST). *Astronomy & Astrophysics* **468**(2):353–377, 2007. <https://doi.org/10.1051/0004-6361:20065724>
- [28] C. J. Lada. Star formation: From OB associations to protostars. In M. Peimbert, J. Jugaku (eds.), *Star Forming Regions*, vol. 115, p. 1. 1987.
- [29] N. A. Webb, M. Coriat, I. Traulsen, et al. The XMM-Newton serendipitous survey. IX. The fourth XMM-Newton serendipitous source catalogue. *Astronomy & Astrophysics* **641**:A136, 2020. <https://doi.org/10.1051/0004-6361/201937353>
- [30] E. W. Flesch. The millions of optical-radio/X-ray associations (MORX) catalogue, v2. *The Open Journal of Astrophysics* **7**, 2024. <https://doi.org/10.21105/astro.2308.01507>
- [31] D. Stern, R. J. Assef, D. J. Benford, et al. Mid-infrared selection of active galactic nuclei with the wide-field infrared survey explorer. I. Characterizing WISE-selected active galactic nuclei in COSMOS. *The Astrophysical Journal* **753**(1):30, 2012. <https://doi.org/10.1088/0004-637X/753/1/30>
- [32] V. S. Pérez-Díaz, J. R. Martínez-Galarza, A. Caicedo, R. D'Abrusco. Unsupervised machine learning for the classification of astrophysical X-ray sources. *Monthly Notices of the Royal Astronomical Society* **528**(3):4852–4871, 2024. <https://doi.org/10.1093/mnras/stae260>
- [33] M. Guedel, K. R. Briggs, K. Arzner, et al. VizieR online data catalog: XMM-Newton extended survey of Taurus: J/A+A/468/353, 2007. <https://doi.org/10.26093/cds/vizier.34680353>
- [34] L. Davis, Jr., J. L. Greenstein. The polarization of starlight by aligned dust grains. *The Astrophysical Journal* **114**:206, 1951. <https://doi.org/10.1086/145464>

- [35] H. Hildebrand, J. A. Davidson, J. L. Dotson, et al. Erratum: A primer on far-infrared polarimetry. *Publications of the Astronomical Society of the Pacific* **112**(778):1621, 2000.
<https://doi.org/10.1086/317728>
- [36] M. Wenger, F. Ochsenbein, D. Egret, et al. The SIMBAD astronomical database. The CDS reference database for astronomical objects. *Astronomy and Astrophysics Supplement Series* **143**:9–22, 2000.
<https://doi.org/10.1051/aas:2000332>
- [37] Bonnarel, F., Fernique, P., Bienaymé, O., et al. The ALADIN interactive sky atlas – A reference tool for identification of astronomical sources. *Astronomy and Astrophysics Supplement Series* **143**(1):33–40, 2000.
<https://doi.org/10.1051/aas:2000331>
- [38] Ochsenbein, F., Bauer, P., Marcout, J. The VizieR database of astronomical catalogues. *Astronomy and Astrophysics Supplement Series* **143**(1):23–32, 2000.
<https://doi.org/10.1051/aas:2000169>

Appendix A.

TABLE 3. Data points on Figure 3 for Haro 6-33 from VizieR Photometry viewer.

λ [μm]	$\nu F(\nu)$ [W m^{-2}]	Error [W m^{-2}]	Vizier table	Vizier ID
0.34	6.88×10^{-17}	5.40×10^{-18}	II/370/xmmom5s	recno=1493997
0.34	6.89×10^{-17}	5.40×10^{-18}	II/356/xmmom41s	recno=1404730
0.35	1.35×10^{-16}	9.37×10^{-18}	J/ApJS/253/19/mstars	recno=45351
0.35	1.37×10^{-16}	9.37×10^{-18}	IV/34/epic	ID=248018164&-c=070.411763 +25.940765,eq=J2000&-c.rs=0.004
0.35	1.41×10^{-16}	1.02×10^{-17}	V/154/sdss16	-c=070.411754 +25.940758,eq=ICRS&-c.rs=0.004
0.35	1.43×10^{-16}	1.02×10^{-17}	I/353/gsc242	-c=070.41180397042 +25.94067833689,eq=ICRS&-c.rs=0.004
0.44	6.36×10^{-16}	9.58×10^{-17}	IV/38/tic	-c=070.41179395162 +25.94078969880,eq=J2000&-c.rs=0.004
0.44	1.05×10^{-15}	4.39×10^{-16}	I/305/out	GSC2.3====N9RV004914&-c=070.411814 +25.940912,eq=J2000&-c.rs=0.00
0.47	8.33×10^{-16}	3.14×10^{-16}	I/305/out	GSC2.3====N9RV004914&-c=070.411814 +25.940912,eq=J2000&-c.rs=0.00
0.48	1.12×10^{-15}	3.14×10^{-17}	II/349/ps1	-c=070.411801850 +25.940684730,eq=J2000&-c.rs=0.004
0.48	1.37×10^{-15}	3.14×10^{-17}	J/AJ/156/241/table4	recno=2882736
0.48	6.47×10^{-16}	6.22×10^{-18}	IV/34/epic	ID=248018164&-c=070.411763 +25.940765,eq=J2000&-c.rs=0.004
0.48	1.11×10^{-15}	3.11×10^{-17}	I/353/gsc242	-c=070.41180397042 +25.94067833689,eq=ICRS&-c.rs=0.004
0.50	2.10×10^{-15}	1.19×10^{-16}	I/350/gaiaedr3	-c=070.41180463045 +25.94067562056,eq=ICRS&-c.rs=0.004
0.50	2.00×10^{-15}	1.90×10^{-16}	I/345/gaia2	-c=070.41180397042 +25.94067833689,eq=ICRS&-c.rs=0.004
0.55	8.61×10^{-16}		J/MNRAS/444/1157/table2	recno=133
0.55	2.67×10^{-15}		II/366/catv2021	recno=518426
0.58	6.80×10^{-15}	1.54×10^{-16}	I/350/gaiaedr3	-c=070.41180463045 +25.94067562056,eq=ICRS&-c.rs=0.004
0.61	4.82×10^{-15}	2.50×10^{-16}	II/349/ps1	-c=070.411801850 +25.940684730,eq=J2000&-c.rs=0.004
0.61	4.94×10^{-15}	$0 \times 10^{+0}$	J/AJ/156/241/table4	recno=2882736
0.62	6.69×10^{-15}	1.44×10^{-16}	I/345/gaia2	-c=070.41180397042 +25.94067833689,eq=ICRS&-c.rs=0.004
0.62	3.48×10^{-15}	1.44×10^{-17}	V/154/sdss16	-c=070.411754 +25.940758,eq=ICRS&-c.rs=0.004
0.62	3.49×10^{-15}	1.44×10^{-17}	J/ApJS/253/19/mstars	recno=45351
0.62	3.50×10^{-15}	1.44×10^{-17}	V/154/sdss16	-c=070.411761 +25.940764,eq=ICRS&-c.rs=0.004
0.62	3.50×10^{-15}	1.44×10^{-17}	IV/34/epic	ID=248018164&-c=070.411763 +25.940765,eq=J2000&-c.rs=0.004
0.62	4.74×10^{-15}	2.45×10^{-16}	I/353/gsc242	-c=070.41180397042 +25.94067833689,eq=ICRS&-c.rs=0.004
0.64	5.81×10^{-15}	2.20×10^{-15}	I/305/out	GSC2.3====N9RV004914&-c=070.411814 +25.940912,eq=J2000&-c.rs=0.00
0.67	1.28×10^{-15}	1.11×10^{-16}	I/353/gsc242	-c=070.41180397042 +25.94067833689,eq=ICRS&-c.rs=0.004
0.67	5.48×10^{-15}		J/AJ/162/110/table1	recno=432
0.67	5.52×10^{-15}	1.34×10^{-16}	II/366/catv2021	recno=518426
0.67	5.66×10^{-15}	1.34×10^{-16}	I/353/gsc242	-c=070.41180397042 +25.94067833689,eq=ICRS&-c.rs=0.004
0.67	9.98×10^{-15}		I/337/gaia	-c=070.4118028781 +25.9406807597,eq=ICRS&-c.rs=0.004
0.67	2.33×10^{-14}	1.60×10^{-15}	I/353/gsc242	-c=070.41180397042 +25.94067833689,eq=ICRS&-c.rs=0.004
0.75	1.06×10^{-14}	1.60×10^{-16}	J/AJ/156/241/table4	recno=2882736
0.75	1.34×10^{-14}	3.21×10^{-16}	II/349/ps1	-c=070.411801850 +25.940684730,eq=J2000&-c.rs=0.004
0.76	1.90×10^{-14}	1.14×10^{-15}	I/350/gaiaedr3	-c=070.41180463045 +25.94067562056,eq=ICRS&-c.rs=0.004
0.76	1.03×10^{-14}	3.93×10^{-17}	V/154/sdss16	-c=070.411754 +25.940758,eq=ICRS&-c.rs=0.004
0.76	1.04×10^{-14}	3.93×10^{-17}	V/154/sdss16	-c=070.411761 +25.940764,eq=ICRS&-c.rs=0.004
0.76	1.04×10^{-14}	3.93×10^{-17}	J/ApJS/253/19/mstars	recno=45351
0.76	1.04×10^{-14}	3.93×10^{-17}	IV/34/epic	ID=248018164&-c=070.411763 +25.940765,eq=J2000&-c.rs=0.004
0.76	1.32×10^{-14}	3.14×10^{-16}	I/353/gsc242	-c=070.41180397042 +25.94067833689,eq=ICRS&-c.rs=0.004

λ [μm]	$\nu F(\nu)$ [W m^{-2}]	Error [W m^{-2}]	Vizier table	Vizier ID
0.77	1.77×10^{-14}	1.32×10^{-15}	I/345/gaia2	-c=070.41180397042 +25.94067833689,eq=ICRS&-c.rs=0.004
0.78	1.34×10^{-14}	5.28×10^{-15}	I/305/out	GSC2.3====N9RV004914&-c=070.411814 +25.940912,eq=J2000&-c.rs=0.00
0.79	5.66×10^{-15}		J/MNRAS/444/1157/table2	recno=133
0.87	1.85×10^{-14}	1.14×10^{-15}	J/AJ/156/241/table4	recno=2882736
0.87	2.62×10^{-14}	4.85×10^{-16}	II/349/ps1	-c=070.411801850 +25.940684730,eq=J2000&-c.rs=0.004
0.88	3.37×10^{-14}	3.40×10^{-17}	II/319/gcs9	-c=070.411794 +25.940742,eq=J2000&-c.rs=0.004
0.90	2.51×10^{-14}	4.65×10^{-16}	I/353/gsc242	-c=070.41180397042 +25.94067833689,eq=ICRS&-c.rs=0.004
0.90	2.59×10^{-14}	9.97×10^{-17}	V/154/sdss16	-c=070.411754 +25.940758,eq=ICRS&-c.rs=0.004
0.90	2.59×10^{-14}	9.97×10^{-17}	V/154/sdss16	-c=070.411761 +25.940764,eq=ICRS&-c.rs=0.004
0.90	2.62×10^{-14}	9.97×10^{-17}	IV/34/epic	ID=248018164&-c=070.411763 +25.940765,eq=J2000&-c.rs=0.004
0.96	3.28×10^{-14}	9.37×10^{-16}	J/AJ/156/241/table4	recno=2882736
0.96	4.69×10^{-14}	2.19×10^{-15}	II/349/ps1	-c=070.411801850 +25.940684730,eq=J2000&-c.rs=0.004
1.03	6.55×10^{-14}	$0 \times 10^{+0}$	II/319/gcs9	-c=070.411794 +25.940742,eq=J2000&-c.rs=0.004
1.24	6.94×10^{-14}		I/297/out	NOMAD1====1159-0059642&-c=070.4117639 +25.9409889,eq=J2000&-c.rs=
1.24	7.02×10^{-14}	1.45×10^{-15}	II/332/c2d	recno=5309093
1.25	1.13×10^{-13}	$0 \times 10^{+0}$	II/319/gcs9	-c=070.411794 +25.940742,eq=J2000&-c.rs=0.004
1.25	7.03×10^{-14}	1.44×10^{-15}	II/246/out	2MASS====04413882+2556267 &-c=070.411763 +25.940765,eq=J2000&-c.r
1.25	7.15×10^{-14}	7.19×10^{-16}	II/246/out	2MASS====04413882+2556267 &-c=070.411763 +25.940765,eq=J2000&-c.r
1.63	1.71×10^{-13}	3.49×10^{-15}	II/246/out	2MASS====04413882+2556267 &-c=070.411763 +25.940765,eq=J2000&-c.r
1.63	1.73×10^{-13}	9.20×10^{-16}	II/246/out	2MASS====04413882+2556267 &-c=070.411763 +25.940765,eq=J2000&-c.r
1.65	1.63×10^{-13}	3.27×10^{-15}	II/368/sstsl2	-c=070.4117764 +25.9407545,eq=J2000&-c.rs=0.004
1.65	1.65×10^{-13}	3.45×10^{-15}	II/332/c2d	recno=5309093
1.65	1.66×10^{-13}		II/338/catalog	recno=38622
1.65	1.70×10^{-13}	3.45×10^{-15}	I/317/sample	PPMXL=3103192842720665194&-c=070.411801 +25.940901,eq=J2000&-c.r
1.65	1.70×10^{-13}		I/297/out	+25.9409889,eq=J2000&-c.rs=
2.16	1.90×10^{-13}	2.77×10^{-15}	II/368/sstsl2	-c=070.4117764 +25.9407545,eq=J2000&-c.rs=0.004
2.16	1.93×10^{-13}	2.77×10^{-15}	II/332/c2d	recno=5309093
2.16	1.95×10^{-13}	2.77×10^{-15}	I/317/sample	PPMXL=3103192842720665194&-c=070.411801 +25.940901,eq=J2000&-c.r
2.19	1.86×10^{-13}	2.74×10^{-15}	II/246/out	2MASS====04413882+2556267 &-c=070.411763 +25.940765,eq=J2000&-c.r
2.19	1.89×10^{-13}	1.37×10^{-15}	II/246/out	2MASS====04413882+2556267 &-c=070.411763 +25.940765,eq=J2000&-c.r
2.20	5.45×10^{-14}	$0 \times 10^{+0}$	II/316/gps6	-c=070.411786 +25.940733,eq=ICRS&-c.rs=0.004
2.20	9.40×10^{-14}		II/319/gcs9	-c=070.411794 +25.940742,eq=J2000&-c.rs=0.004
2.20	1.59×10^{-13}		II/316/gps6	-c=070.411786 +25.940733,eq=ICRS&-c.rs=0.004
2.20	2.08×10^{-13}		II/316/gps6	-c=070.411786 +25.940733,eq=ICRS&-c.rs=0.004
3.35	1.40×10^{-13}	2.68×10^{-15}	II/365/catwise	-c=070.4118218 +25.9406836,eq=ICRS&-c.rs=0.004
3.35	1.45×10^{-13}	2.68×10^{-15}	II/368/sstsl2	-c=070.4117764 +25.9407545,eq=J2000&-c.rs=0.004
3.35	1.47×10^{-13}	2.68×10^{-15}	I/353/gsc242	-c=070.41180397042 +25.94067833689,eq=ICRS&-c.rs=0.004
3.35	1.49×10^{-13}	$0 \times 10^{+0}$	II/363/unwise	-c=070.4118104 +25.9407152,eq=J2000&-c.rs=0.004
3.35	1.50×10^{-13}		II/338/catalog	recno=38622
3.35	1.51×10^{-13}	3.58×10^{-15}	II/311/wise	WISE====J044138.82+255626.7&-c=070.411789 +25.940759,eq=J2000&-c.
3.55	9.80×10^{-14}	6.76×10^{-15}	II/332/c2d	recno=5309093
3.55	1.20×10^{-13}	5.91×10^{-15}	J/ApJS/186/259/known	recno=206
3.55	1.25×10^{-13}	2.53×10^{-15}	J/ApJ/784/126/table1	recno=346
4.49	9.61×10^{-14}	4.67×10^{-15}	J/ApJS/186/259/known	recno=206
4.49	1.06×10^{-13}	6.01×10^{-15}	II/332/c2d	recno=5309093
4.49	1.08×10^{-13}	2.00×10^{-15}	J/ApJ/784/126/table1	recno=346
4.60	1.15×10^{-13}	1.30×10^{-15}	II/365/catwise	-c=070.4118218 +25.9406836,eq=ICRS&-c.rs=0.004

λ [μm]	$\nu F(\nu)$ [W m^{-2}]	Error [W m^{-2}]	Vizier table	Vizier ID
4.60	1.19×10^{-13}	$0 \times 10^{+0}$	II/363/unwise	-c=070.4118104 +25.9407152,eq=J2000&-c.rs=0.004
4.60	1.23×10^{-13}	1.96×10^{-15}	II/368/sstsl2	-c=070.4117764 +25.9407545,eq=J2000&-c.rs=0.004
4.60	1.25×10^{-13}	1.96×10^{-15}	I/353/gsc242	-c=070.41180397042 +25.94067833689,eq=ICRS&-c.rs=0.004
4.60	1.27×10^{-13}	1.96×10^{-15}	II/311/wise	WISE====J044138.82+255626.7&-c=070.411789+25.9407595,eq=J2000&-c.
4.60	1.28×10^{-13}	2.61×10^{-15}	J/ApJ/784/126/table1	recno=346
4.60	1.28×10^{-13}		II/338/catalog	recno=38622
5.73	8.47×10^{-14}	3.66×10^{-15}	J/ApJS/186/259/known	recno=206
5.73	9.73×10^{-14}	2.62×10^{-15}	J/ApJ/784/126/table1	recno=346
5.73	1.06×10^{-13}	$0 \times 10^{+0}$	II/368/sstsl2	-c=070.4117764 +25.9407545,eq=J2000&-c.rs=0.004
5.73	1.30×10^{-13}	6.28×10^{-15}	II/332/c2d	recno=5309093
7.87	9.29×10^{-14}	4.19×10^{-15}	J/ApJS/186/259/known	recno=206
7.87	1.01×10^{-13}	2.67×10^{-15}	J/ApJ/784/126/table1	recno=346
7.87	1.07×10^{-13}	$0 \times 10^{+0}$	II/368/sstsl2	-c=070.4117764 +25.9407545,eq=J2000&-c.rs=0.004
7.87	1.61×10^{-13}	9.90×10^{-15}	II/332/c2d	recno=5309093
8.61	1.25×10^{-13}	4.87×10^{-15}	II/338/catalog	recno=38622
11.56	1.11×10^{-13}	1.04×10^{-15}	J/AJ/158/54/table1	recno=414
11.56	1.11×10^{-13}	1.30×10^{-15}	II/328/allwise	AllWISE====J044138.83+255626.6&-c=070.4117932 +25.9407276,eq=J200
11.56	1.11×10^{-13}	1.30×10^{-15}	I/353/gsc242	-c=070.41180397042 +25.94067833689,eq=ICRS&-c.rs=0.004
11.56	1.12×10^{-13}	1.04×10^{-15}	J/ApJ/784/126/table1	recno=346
11.56	1.12×10^{-13}	1.30×10^{-15}	II/311/wise	WISE====J044138.82+255626.7&-c=070.411789+25.9407595,eq=J2000&-c.
11.56	1.19×10^{-13}	1.30×10^{-15}	II/368/sstsl2	-c=070.4117764 +25.9407545,eq=J2000&-c.rs=0.004
11.56	1.23×10^{-13}		II/338/catalog	recno=38622
11.59	1.40×10^{-13}		II/338/catalog	recno=38622
11.59	1.48×10^{-13}		II/338/catalog	recno=38622
18.39	1.56×10^{-13}	5.22×10^{-15}	II/338/catalog	recno=38622
22.09	1.72×10^{-13}	2.71×10^{-15}	II/368/sstsl2	-c=070.4117764 +25.9407545,eq=J2000&-c.rs=0.004
22.09	1.75×10^{-13}	2.71×10^{-15}	I/353/gsc242	-c=070.41180397042 +25.94067833689,eq=ICRS&-c.rs=0.004
22.09	1.76×10^{-13}	1.36×10^{-15}	J/ApJ/784/126/table1	recno=346
22.09	1.78×10^{-13}	2.71×10^{-15}	II/311/wise	WISE====J044138.82+255626.7&-c=070.411789+25.9407595,eq=J2000&-c.
22.09	1.79×10^{-13}		II/338/catalog	recno=38622
23.67	1.61×10^{-13}	1.52×10^{-14}	II/332/c2d	recno=5309093
23.67	1.63×10^{-13}	6.33×10^{-15}	J/ApJ/784/126/table1	recno=346
23.67	1.67×10^{-13}	$0 \times 10^{+0}$	II/368/sstsl2	-c=070.4117764 +25.9407545,eq=J2000&-c.rs=0.004
23.67	6.46×10^{-12}	2.41×10^{-13}	J/ApJ/836/34/table2	recno=780
23.88	1.91×10^{-13}		II/338/catalog	recno=38622
23.88	1.95×10^{-13}		II/338/catalog	recno=38622
61.85	1.33×10^{-13}		II/338/catalog	recno=38622
61.85	1.40×10^{-13}		II/338/catalog	recno=38622
70.00	1.23×10^{-13}	2.14×10^{-15}	J/A+A/688/A203/bshrcds	recno=5342
70.00	1.24×10^{-13}	2.57×10^{-14}	J/ApJ/849/63/ysos	recno=109
71.42	7.47×10^{-14}	1.51×10^{-14}	J/ApJS/186/259/known	recno=206
71.42	8.86×10^{-14}	8.40×10^{-15}	II/332/c2d	recno=5309093
100.00	8.99×10^{-14}	1.80×10^{-14}	J/ApJ/849/63/ysos	recno=109
101.95	1.71×10^{-13}		II/338/catalog	recno=38622
101.95	2.36×10^{-13}		II/338/catalog	recno=38622
155.90	3.79×10^{-14}	7.69×10^{-15}	J/ApJS/186/259/known	recno=206
160.00	4.87×10^{-14}	9.37×10^{-15}	J/ApJ/849/63/ysos	recno=109
249.99	1.56×10^{-14}	3.60×10^{-15}	J/ApJ/849/63/ysos	recno=109
249.99	1.73×10^{-14}	3.60×10^{-16}	VIII/112/spsc250	recno=263696
249.99	1.75×10^{-14}	2.40×10^{-16}	VIII/112/spsc250	recno=263696
249.99	1.93×10^{-14}	2.40×10^{-16}	VIII/112/spsc250	recno=263696
249.99	1.95×10^{-14}	3.60×10^{-16}	VIII/112/spsc250	recno=263696
363.00	5.78×10^{-15}	8.26×10^{-16}	J/ApJ/849/63/ysos	recno=109
886.96	2.00×10^{-16}	2.84×10^{-17}	J/ApJ/771/129/table2	recno=171
1300.00	5.88×10^{-17}	5.07×10^{-18}	J/ApJ/872/158/table4	recno=176
1332.41	5.74×10^{-17}	4.95×10^{-18}	J/ApJ/771/129/table2	recno=171

TABLE 4. Data points on Figure 4 for JH 223 from VizieR Photometry viewer.

λ [μm]	$\nu F(\nu)$ [W m^{-2}]	Error [W m^{-2}]	Vizier table	Vizier ID
0.34	6.83×10^{-16}	1.13×10^{-17}	II/370/xmmom5s	recno=1493547
0.34	6.84×10^{-16}	1.13×10^{-17}	II/356/xmmom41s	recno=1404279
0.35	8.49×10^{-16}	1.62×10^{-17}	V/154/sdss16	-c=070.206253 +25.855252,eq=ICRS&-c.rs=0.004
0.35	8.60×10^{-16}	1.70×10^{-17}	I/353/gsc242	-c=070.20631586592 +25.85518403387,eq=ICRS&-c.rs=0.004
0.35	8.69×10^{-16}	1.70×10^{-17}	IV/38/tic	-c=070.20629490024 +25.85526855322,eq=J2000&-c.rs=0.004
0.35	9.80×10^{-16}	1.70×10^{-17}	V/154/sdss16	-c=070.206253 +25.855252,eq=ICRS&-c.rs=0.004
0.35	9.88×10^{-16}	1.70×10^{-17}	V/154/sdss16	-c=070.206247 +25.855259,eq=ICRS&-c.rs=0.004
0.40	2.08×10^{-13}		I/358/varisum	-c= 70.20631650736 +25.85518131742,eq=ICRS&-c.rs=0.004
0.44	2.96×10^{-15}	1.23×10^{-15}	I/305/out	GSC2.3==N9RV000756&-c=070.206325 +25.855384,eq=J2000&-c.rs=0.00
0.44	5.43×10^{-15}		II/336/apass9	-c=070.206175 +25.855062,eq=J2000&-c.rs=0.004
0.47	6.02×10^{-15}	2.33×10^{-15}	I/305/out	GSC2.3==N9RV000756&-c=070.206325 +25.855384,eq=J2000&-c.rs=0.00
0.48	7.10×10^{-15}		J/AJ/156/241/table4	recno=2879389
0.48	7.73×10^{-15}	1.26×10^{-16}	II/349/ps1	-c=070.206312620 +25.855188720,eq=J2000&-c.rs=0.004
0.48	5.47×10^{-15}	2.49×10^{-17}	IV/38/tic	-c=070.20629490024 +25.85526855322,eq=J2000&-c.rs=0.004
0.48	5.48×10^{-15}	2.49×10^{-17}	V/154/sdss16	-c=070.206253 +25.855252,eq=ICRS&-c.rs=0.004
0.48	6.16×10^{-15}	2.49×10^{-17}	V/154/sdss16	-c=070.206253 +25.855252,eq=ICRS&-c.rs=0.004
0.48	6.18×10^{-15}	2.49×10^{-17}	V/154/sdss16	-c=070.206247 +25.855259,eq=ICRS&-c.rs=0.004
0.48	7.21×10^{-15}	5.60×10^{-16}	II/336/apass9	-c=070.206175 +25.855062,eq=J2000&-c.rs=0.004
0.48	7.71×10^{-15}	1.24×10^{-16}	I/353/gsc242	-c=070.20631586592 +25.85518403387,eq=ICRS&-c.rs=0.004
0.50	1.08×10^{-14}	2.38×10^{-16}	I/350/gaiaedr3	-c=070.20631650736 +25.85518131742,eq=ICRS&-c.rs=0.004
0.50	1.04×10^{-14}	2.97×10^{-16}	I/345/gaia2	-c=070.20631586592 +25.85518403387,eq=ICRS&-c.rs=0.004
0.55	8.61×10^{-15}	1.73×10^{-15}	IV/38/tic	-c=070.20629490024 +25.85526855322,eq=J2000&-c.rs=0.004
0.55	1.33×10^{-14}		II/336/apass9	-c=070.206175 +25.855062,eq=J2000&-c.rs=0.004
0.58	3.82×10^{-14}	2.57×10^{-16}	I/350/gaiaedr3	-c=070.20631650736 +25.85518131742,eq=ICRS&-c.rs=0.004
0.61	2.38×10^{-14}		J/AJ/156/241/table4	recno=2879389
0.61	2.47×10^{-14}	1.47×10^{-16}	II/349/ps1	-c=070.206312620 +25.855188720,eq=J2000&-c.rs=0.004
0.62	3.51×10^{-14}	2.89×10^{-16}	I/345/gaia2	-c=070.20631586592 +25.85518403387,eq=ICRS&-c.rs=0.004
0.62	2.22×10^{-14}	9.60×10^{-17}	V/154/sdss16	-c=070.206253 +25.855252,eq=ICRS&-c.rs=0.004
0.62	2.23×10^{-14}	9.60×10^{-17}	V/154/sdss16	-c=070.206247 +25.855259,eq=ICRS&-c.rs=0.004
0.62	2.43×10^{-14}	1.44×10^{-16}	I/353/gsc242	-c=070.20631586592 +25.85518403387,eq=ICRS&-c.rs=0.004
0.62	2.46×10^{-14}	1.44×10^{-16}	IV/38/tic	-c=070.20629490024 +25.85526855322,eq=J2000&-c.rs=0.004
0.62	2.58×10^{-14}	8.64×10^{-16}	II/336/apass9	-c=070.206175 +25.855062,eq=J2000&-c.rs=0.004
0.64	3.07×10^{-14}	1.19×10^{-14}	I/305/out	GSC2.3==N9RV000756&-c=070.206325 +25.855384,eq=J2000&-c.rs=0.00
0.67	2.28×10^{-15}		J/AJ/166/218/table1	recno=22809
0.67	6.68×10^{-15}	1.78×10^{-16}	I/353/gsc242	-c=070.20631586592 +25.85518403387,eq=ICRS&-c.rs=0.004
0.67	6.82×10^{-15}		J/AJ/166/218/table1	recno=22809
0.67	2.97×10^{-14}		J/ApJ/917/23/table2	recno=27491
0.67	2.97×10^{-14}	2.23×10^{-16}	I/353/gsc242	-c=070.20631586592 +25.85518403387,eq=ICRS&-c.rs=0.004
0.67	3.08×10^{-14}		J/ApJ/917/23/table1	recno=28207
0.67	3.08×10^{-14}		III/286/catalog	recno=108605
0.67	3.55×10^{-14}		I/337/gaia	-c=070.2063157402 +25.8551866093,eq=ICRS&-c.rs=0.004
0.67	9.49×10^{-14}	2.23×10^{-15}	I/353/gsc242	-c=070.20631586592 +25.85518403387,eq=ICRS&-c.rs=0.004
0.67	9.76×10^{-14}		J/AJ/166/218/table1	recno=22809
0.75	4.21×10^{-14}		J/AJ/156/241/table4	recno=2879389
0.75	5.93×10^{-14}		II/349/ps1	-c=070.206312620 +25.855188720,eq=J2000&-c.rs=0.004
0.76	7.28×10^{-14}	1.57×10^{-15}	I/350/gaiaedr3	-c=070.20631650736 +25.85518131742,eq=ICRS&-c.rs=0.004

λ [μm]	$\nu F(\nu)$ [W m^{-2}]	Error [W m^{-2}]	Vizier table	Vizier ID
0.76	6.01×10^{-14}	3.93×10^{-16}	V/154/sdss16	-c=070.206253 +25.855252,eq=ICRS&-c.rs=0.004
0.76	6.05×10^{-14}	3.93×10^{-16}	V/154/sdss16	-c=070.206247 +25.855259,eq=ICRS&-c.rs=0.004
0.76	6.83×10^{-14}	3.93×10^{-16}	IV/38/tic	-c=070.20629490024 +25.85526855322,eq=J2000&-c.rs=0.004
0.76	8.05×10^{-14}	4.32×10^{-15}	II/336/apass9	-c=070.206175 +25.855062,eq=J2000&-c.rs=0.004
0.77	7.18×10^{-14}	1.94×10^{-15}	I/345/gaia2	-c=070.20631586592 +25.85518403387,eq=ICRS&-c.rs=0.004
0.78	1.22×10^{-13}	4.82×10^{-14}	I/305/out	GSC2.3====N9RV000756&-c=070.206325 +25.855384,eq=J2000&-c.rs=0.00
0.87	6.44×10^{-14}		J/AJ/156/241/table4	recno=2879389
0.87	1.03×10^{-13}		II/349/ps1	-c=070.206312620 +25.855188720,eq=J2000&-c.rs=0.004
0.88	1.08×10^{-13}	$0 \times 10^{+0}$	II/319/gcs9	-c=070.206305 +25.855240,eq=J2000&-c.rs=0.004
0.90	1.12×10^{-13}	3.32×10^{-16}	V/154/sdss16	-c=070.206253 +25.855252,eq=ICRS&-c.rs=0.004
0.90	1.13×10^{-13}	3.32×10^{-16}	J/ApJS/253/19/mstars	recno=334526
0.90	1.14×10^{-13}	3.32×10^{-16}	IV/38/tic	-c=070.20629490024 +25.85526855322,eq=J2000&-c.rs=0.004
0.90	1.17×10^{-13}	3.32×10^{-16}	V/154/sdss16	-c=070.206247 +25.855259,eq=ICRS&-c.rs=0.004
0.90	1.19×10^{-13}	3.32×10^{-16}	V/154/sdss16	-c=070.206253 +25.855252,eq=ICRS&-c.rs=0.004
0.96	7.84×10^{-14}		J/AJ/156/241/table4	recno=2879389
0.96	1.28×10^{-13}	4.69×10^{-15}	II/349/ps1	-c=070.206312620 +25.855188720,eq=J2000&-c.rs=0.004
1.03	1.17×10^{-13}	$0 \times 10^{+0}$	II/319/gcs9	-c=070.206305 +25.855240,eq=J2000&-c.rs=0.004
1.24	1.91×10^{-13}	4.11×10^{-15}	II/368/sstsl2	-c=070.2062531 +25.8553357,eq=J2000&-c.rs=0.004
1.24	1.91×10^{-13}		I/297/out	NOMAD1====1158-0059949&-c=070.2062519 +25.8552747,eq=J2000&-c.rs=
1.24	1.93×10^{-13}	4.11×10^{-15}	II/332/c2d	recno=5236589
1.25	1.35×10^{-13}	2.40×10^{-16}	II/319/gcs9	-c=070.206305 +25.855240,eq=J2000&-c.rs=0.004
1.25	1.94×10^{-13}	4.08×10^{-15}	II/246/out	2MASS====04404950+2551191 &-c=070.206284 +25.855328,eq=J2000&-c.r
1.25	2.06×10^{-13}	2.16×10^{-15}	II/246/out	2MASS====04404950+2551191 &-c=070.206284 +25.855328,eq=J2000&-c.r
1.63	2.06×10^{-13}	5.52×10^{-15}	II/246/out	2MASS====04404950+2551191 &-c=070.206284 +25.855328,eq=J2000&-c.r
1.63	2.17×10^{-13}	3.68×10^{-15}	II/246/out	2MASS====04404950+2551191 &-c=070.206284 +25.855328,eq=J2000&-c.r
1.65	1.96×10^{-13}	5.45×10^{-15}	II/368/sstsl2	-c=070.2062531 +25.8553357,eq=J2000&-c.rs=0.004
1.65	2.00×10^{-13}	5.45×10^{-15}	II/332/c2d	recno=5236589
1.65	2.05×10^{-13}		I/297/out	NOMAD1====1158-0059949&-c=070.2062519 +25.8552747,eq=J2000&-c.rs=
2.16	1.45×10^{-13}	2.77×10^{-15}	II/368/sstsl2	-c=070.2062531 +25.8553357,eq=J2000&-c.rs=0.004
2.16	1.47×10^{-13}	2.77×10^{-15}	II/332/c2d	recno=5236589
2.16	1.50×10^{-13}	2.77×10^{-15}	I/317/sample	PPMXL=3103050302883991366&-c=070.206291 +25.855327,eq=J2000&-c.r
2.19	1.42×10^{-13}	2.74×10^{-15}	II/246/out	2MASS====04404950+2551191 &-c=070.206284 +25.855328,eq=J2000&-c.r
2.19	1.46×10^{-13}	1.37×10^{-15}	II/246/out	2MASS====04404950+2551191 &-c=070.206284 +25.855328,eq=J2000&-c.r
2.20	1.04×10^{-13}	1.36×10^{-16}	II/316/gps6	-c=070.206302 +25.855240,eq=ICRS&-c.rs=0.004
2.20	1.16×10^{-13}		II/316/gps6	-c=070.206302 +25.855240,eq=ICRS&-c.rs=0.004
2.20	1.17×10^{-13}		II/316/gps6	-c=070.206302 +25.855240,eq=ICRS&-c.rs=0.004
3.35	7.19×10^{-14}	$0 \times 10^{+0}$	II/363/unwise	-c=070.2062786 +25.8552530,eq=J2000&-c.rs=0.004
3.35	7.19×10^{-14}	1.52×10^{-15}	II/368/sstsl2	-c=070.2062531 +25.8553357,eq=J2000&-c.rs=0.004
3.35	7.23×10^{-14}	8.05×10^{-16}	II/365/catwise	-c=070.2062953 +25.8552378,eq=ICRS&-c.rs=0.004
3.35	7.28×10^{-14}	1.34×10^{-15}	J/AJ/158/54/table1	recno=404
3.35	7.29×10^{-14}	1.52×10^{-15}	I/353/gsc242	-c=070.20631586592 +25.85518403387,eq=ICRS&-c.rs=0.004
3.35	7.55×10^{-14}	1.43×10^{-15}	J/ApJ/784/126/table1	recno=338
3.35	7.60×10^{-14}	1.61×10^{-15}	II/311/wise	WISE====J044049.50+255119.0&-c=070.206275 +25.855304,eq=J2000&-c.r
3.55	4.57×10^{-14}	$0 \times 10^{+0}$	II/368/sstsl2	-c=070.2062531 +25.8553357,eq=J2000&-c.rs=0.004
3.55	5.65×10^{-14}	4.39×10^{-15}	II/332/c2d	recno=5236589
3.55	6.51×10^{-14}	3.04×10^{-15}	J/ApJS/186/259/known	recno=200
3.55	6.76×10^{-14}	1.27×10^{-15}	J/ApJ/784/126/table1	recno=338
4.49	3.07×10^{-14}	$0 \times 10^{+0}$	II/368/sstsl2	-c=070.2062531 +25.8553357,eq=J2000&-c.rs=0.004
4.49	4.28×10^{-14}	2.87×10^{-15}	II/332/c2d	recno=5236589
4.49	4.35×10^{-14}	2.00×10^{-15}	J/ApJS/186/259/known	recno=200
4.49	4.64×10^{-14}	8.67×10^{-16}	J/ApJ/784/126/table1	recno=338
4.60	4.29×10^{-14}	$0 \times 10^{+0}$	II/363/unwise	-c=070.2062786 +25.8552530,eq=J2000&-c.rs=0.004
4.60	4.43×10^{-14}	3.91×10^{-16}	II/365/catwise	-c=070.2062953 +25.8552378,eq=ICRS&-c.rs=0.004
4.60	4.46×10^{-14}	8.47×10^{-16}	II/368/sstsl2	-c=070.2062531 +25.8553357,eq=J2000&-c.rs=0.004

λ [μm]	$\nu F(\nu)$ [Wm^{-2}]	Error [Wm^{-2}]	Vizier table	Vizier ID
4.60	4.54×10^{-14}	8.47×10^{-16}	I/353/gsc242	-c=070.20631586592 +25.85518403387,eq=ICRS&-c.rs=0.004
4.60	4.55×10^{-14}	8.47×10^{-16}	J/AJ/158/54/table1	recno=404
4.60	4.72×10^{-14}	8.47×10^{-16}	J/ApJ/784/126/table1	recno=338
4.60	4.74×10^{-14}	9.12×10^{-16}	II/311/wise	WISE==J044049.50+255119.0&-c=070.206275 +25.855304,eq=J2000&-c.
5.73	2.90×10^{-14}	1.73×10^{-15}	II/332/c2d	recno=5236589
5.73	2.92×10^{-14}	$0 \times 10^{+0}$	II/368/sstsl2	-c=070.2062531 +25.8553357,eq=J2000&-c.rs=0.004
5.73	2.93×10^{-14}	7.85×10^{-16}	J/ApJ/784/126/table1	recno=338
5.73	3.04×10^{-14}	1.41×10^{-15}	J/ApJS/186/259/known	recno=200
7.87	1.96×10^{-14}	9.14×10^{-16}	J/ApJS/186/259/known	recno=200
7.87	1.97×10^{-14}	$0 \times 10^{+0}$	II/368/sstsl2	-c=070.2062531 +25.8553357,eq=J2000&-c.rs=0.004
7.87	2.01×10^{-14}	5.71×10^{-16}	J/ApJ/784/126/table1	recno=338
7.87	2.07×10^{-14}	1.07×10^{-15}	II/332/c2d	recno=5236589
11.56	1.09×10^{-14}	1.82×10^{-16}	I/353/gsc242	-c=070.20631586592 +25.85518403387,eq=ICRS&-c.rs=0.004
11.56	1.09×10^{-14}	1.56×10^{-16}	II/311/wise	WISE==J044049.50+255119.0&-c=070.206275 +25.855304,eq=J2000&-c.
11.56	1.10×10^{-14}	2.07×10^{-16}	J/ApJ/784/126/table1	recno=338
11.56	1.16×10^{-14}	1.82×10^{-16}	II/368/sstsl2	-c=070.2062531 +25.8553357,eq=J2000&-c.rs=0.004
22.09	8.59×10^{-15}	3.12×10^{-16}	II/368/sstsl2	-c=070.2062531 +25.8553357,eq=J2000&-c.rs=0.004
22.09	8.70×10^{-15}	3.26×10^{-16}	J/AJ/158/54/table1	recno=404
22.09	8.73×10^{-15}	3.26×10^{-16}	II/328/allwise	AllWISE==J044049.50+255119.0&-c=070.2062877 +25.8552863,eq=J200
22.09	8.74×10^{-15}	3.26×10^{-16}	I/353/gsc242	-c=070.20631586592 +25.85518403387,eq=ICRS&-c.rs=0.004
22.09	8.86×10^{-15}	2.99×10^{-16}	II/311/wise	WISE==J044049.50+255119.0&-c=070.206275 +25.855304,eq=J2000&-c.
23.67	7.07×10^{-15}	6.84×10^{-16}	II/332/c2d	recno=5236589
23.67	7.67×10^{-15}	1.27×10^{-17}	II/368/sstsl2	-c=070.2062531 +25.8553357,eq=J2000&-c.rs=0.004
23.67	7.74×10^{-15}	2.79×10^{-16}	J/ApJ/784/126/table1	recno=338
23.67	8.02×10^{-15}	2.91×10^{-16}	J/ApJS/186/259/known	recno=200
23.67	3.06×10^{-13}	1.14×10^{-14}	J/ApJ/836/34/table2	recno=772
70.00	5.14×10^{-15}	8.57×10^{-16}	J/ApJ/849/63/ysos	recno=119
71.42	4.28×10^{-15}	8.81×10^{-16}	J/ApJS/186/259/known	recno=200
100.00	2.40×10^{-15}	6.00×10^{-16}	J/ApJ/849/63/ysos	recno=119
155.90	1.30×10^{-15}		J/ApJS/186/259/known	recno=200
849.27	2.47×10^{-17}		J/ApJ/773/168/table1	recno=109
880.01	2.38×10^{-17}		J/ApJ/751/115/table6	recno=88
886.96	2.37×10^{-17}		J/ApJ/771/129/table2	recno=165
1300.00	1.75×10^{-18}	3.00×10^{-19}	J/ApJ/872/158/table4	recno=171
1300.00	2.54×10^{-18}	2.77×10^{-19}	J/ApJ/872/158/table2	recno=45
1300.00	3.92×10^{-18}	3.23×10^{-19}	J/ApJ/872/158/table4	recno=170
1300.00	4.38×10^{-17}		J/ApJ/773/168/table1	recno=109
1332.41	3.78×10^{-18}	6.75×10^{-19}	J/A+A/663/A98/tableg1	recno=26
1332.41	6.08×10^{-18}		J/ApJ/771/129/table2	recno=165

TABLE 5. Data points on Figure 5 for XEST 07-024 from VizieR Photometry viewer.

λ [μm]	$\nu F(\nu)$ [Wm^{-2}]	Error [Wm^{-2}]	Vizier table	Vizier ID
0.35	1.69×10^{-17}	5.11×10^{-18}	V/154/sdss16	-c=070.285107 +25.562459,eq=ICRS&-c.rs=0.004
0.35	1.70×10^{-17}	5.20×10^{-18}	IV/34/epic	ID=247966607&-c=070.285121 +25.562456,eq=J2000&-c.rs=0.004
0.35	1.71×10^{-17}	5.20×10^{-18}	I/353/gsc242	-c=070.28496069846 +25.56243415687,eq=ICRS&-c.rs=0.004
0.35	2.26×10^{-17}	5.37×10^{-18}	V/154/sdss16	-c=070.285115 +25.562460,eq=ICRS&-c.rs=0.004
0.48	9.11×10^{-17}	1.01×10^{-17}	II/349/ps1	-c=070.284973280 +25.562431930,eq=J2000&-c.rs=0.004
0.48	4.63×10^{-17}	2.18×10^{-18}	V/154/sdss16	-c=070.285107 +25.562459,eq=ICRS&-c.rs=0.004
0.48	4.65×10^{-17}	2.24×10^{-18}	IV/34/epic	ID=247966607&-c=070.285121 +25.562456,eq=J2000&-c.rs=0.004
0.48	4.76×10^{-17}	2.24×10^{-18}	V/154/sdss16	-c=070.285115 +25.562460,eq=ICRS&-c.rs=0.004
0.48	9.02×10^{-17}	9.95×10^{-18}	I/353/gsc242	-c=070.28496069846 +25.56243415687,eq=ICRS&-c.rs=0.004
0.50	1.97×10^{-16}	1.01×10^{-17}	I/350/gaiadr3	-c=070.28495543413 +25.56243428514,eq=ICRS&-c.rs=0.004
0.50	1.97×10^{-16}	1.01×10^{-17}	I/355/gaiadr3	-c=070.28495543413 +25.56243428514,eq=ICRS&-c.rs=0.004

λ [nm]	$\nu F(\nu)$ [Wm $^{-2}$]	Error [Wm $^{-2}$]	Vizier table	Vizier ID
0.50	2.03×10^{-16}	8.32×10^{-18}	I/345/gaia2	-c=070.28496069846 +25.56243415687,eq=ICRS&-c.rs=0.004
0.58	1.19×10^{-15}	5.15×10^{-18}	I/350/gaiaedr3	-c=070.28495543413 +25.56243428514,eq=ICRS&-c.rs=0.004
0.58	1.23×10^{-15}	5.15×10^{-18}	I/355/gaiadr3	-c=070.28495543413 +25.56243428514,eq=ICRS&-c.rs=0.004
0.61	5.63×10^{-16}	4.89×10^{-18}	II/349/ps1	-c=070.284973280 +25.562431930,eq=J2000&-c.rs=0.004
0.62	1.13×10^{-15}	$0 \times 10^{+0}$	I/345/gaia2	-c=070.28496069846 +25.56243415687,eq=ICRS&-c.rs=0.004
0.62	5.18×10^{-16}	4.80×10^{-18}	IV/34/epic	ID=247966607&-c=070.285121 +25.562456,eq=J2000&-c.rs=0.004
0.62	5.18×10^{-16}	4.80×10^{-18}	V/154/sdss16	-c=070.285107 +25.562459,eq=ICRS&-c.rs=0.004
0.62	5.23×10^{-16}	4.80×10^{-18}	V/154/sdss16	-c=070.285115 +25.562460,eq=ICRS&-c.rs=0.004
0.62	5.52×10^{-16}	4.80×10^{-18}	I/353/gsc242	-c=070.28496069846 +25.56243415687,eq=ICRS&-c.rs=0.004
0.67	1.30×10^{-16}	4.90×10^{-18}	I/353/gsc242	-c=070.28496069846 +25.56243415687,eq=ICRS&-c.rs=0.004
0.67	1.30×10^{-16}	4.90×10^{-18}	J/ApJ/867/105/refcat2	-c=070.28496070 +25.56243416,eq=ICRS&-c.rs=0.004
0.67	9.31×10^{-16}		J/ApJ/917/23/table1	recno=30496
0.67	9.58×10^{-16}	$0 \times 10^{+0}$	I/353/gsc242	-c=070.28496069846 +25.56243415687,eq=ICRS&-c.rs=0.004
0.67	9.58×10^{-16}	$0 \times 10^{+0}$	IV/38/tic	-c=070.28512515484 +25.56243094699,eq=J2000&-c.rs=0.004
0.67	9.58×10^{-16}	$0 \times 10^{+0}$	IV/39/tic82	-c=070.28512515484 +25.56243094699,eq=J2000&-c.rs=0.004
0.67	9.58×10^{-16}	$0 \times 10^{+0}$	J/ApJ/867/105/refcat2	-c=070.28496070 +25.56243416,eq=ICRS&-c.rs=0.004
0.67	1.21×10^{-15}		I/337/gaia	-c=070.2849710755 +25.5624316983,eq=ICRS&-c.rs=0.004
0.67	1.21×10^{-15}	8.91×10^{-18}	I/339/hsoy	-c=070.2849441512 +25.5624735697,eq=J2000&-c.rs=0.004
0.67	1.21×10^{-15}	8.91×10^{-18}	I/339/hsoy	-c=070.2851234416 +25.5624466616,eq=J2000&-c.rs=0.004
0.67	3.55×10^{-15}	1.78×10^{-17}	J/ApJ/867/105/refcat2	-c=070.28496070 +25.56243416,eq=ICRS&-c.rs=0.004
0.67	3.56×10^{-15}	1.78×10^{-17}	I/353/gsc242	-c=070.28496069846 +25.56243415687,eq=ICRS&-c.rs=0.004
0.75	1.98×10^{-15}	4.01×10^{-18}	II/349/ps1	-c=070.284973280 +25.562431930,eq=J2000&-c.rs=0.004
0.76	2.64×10^{-15}	1.57×10^{-17}	I/350/gaiaedr3	-c=070.28495543413 +25.56243428514,eq=ICRS&-c.rs=0.004
0.76	2.64×10^{-15}	1.57×10^{-17}	I/355/gaiadr3	-c=070.28495543413 +25.56243428514,eq=ICRS&-c.rs=0.004
0.76	1.92×10^{-15}	1.18×10^{-17}	V/154/sdss16	-c=070.285107 +25.562459,eq=ICRS&-c.rs=0.004
0.76	1.93×10^{-15}	1.18×10^{-17}	V/154/sdss16	-c=070.285115 +25.562460,eq=ICRS&-c.rs=0.004
0.76	1.94×10^{-15}	1.18×10^{-17}	IV/34/epic	ID=247966607&-c=070.285121 +25.562456,eq=J2000&-c.rs=0.004
0.76	1.95×10^{-15}	3.93×10^{-18}	I/353/gsc242	-c=070.28496069846 +25.56243415687,eq=ICRS&-c.rs=0.004
0.77	2.69×10^{-15}	1.55×10^{-17}	I/345/gaia2	-c=070.28496069846 +25.56243415687,eq=ICRS&-c.rs=0.004
0.87	4.12×10^{-15}	$0 \times 10^{+0}$	II/349/ps1	-c=070.284973280 +25.562431930,eq=J2000&-c.rs=0.004
0.88	4.45×10^{-15}	$0 \times 10^{+0}$	II/319/gcs9	-c=070.285011 +25.562462,eq=J2000&-c.rs=0.004
0.90	3.96×10^{-15}	$0 \times 10^{+0}$	I/353/gsc242	-c=070.28496069846 +25.56243415687,eq=ICRS&-c.rs=0.004
0.90	4.92×10^{-15}	3.32×10^{-17}	V/154/sdss16	-c=070.285115 +25.562460,eq=ICRS&-c.rs=0.004
0.90	4.92×10^{-15}	3.32×10^{-17}	V/154/sdss16	-c=070.285107 +25.562459,eq=ICRS&-c.rs=0.004
0.90	4.95×10^{-15}	3.32×10^{-17}	IV/34/epic	ID=247966607&-c=070.285121 +25.562456,eq=J2000&-c.rs=0.004
0.96	6.59×10^{-15}	3.12×10^{-17}	II/349/ps1	-c=070.284973280 +25.562431930,eq=J2000&-c.rs=0.004
1.03	7.74×10^{-15}	2.91×10^{-17}	II/319/gcs9	-c=070.285011 +25.562462,eq=J2000&-c.rs=0.004
1.24	1.27×10^{-14}	2.90×10^{-16}	II/368/ssstsl2	-c=070.2850393 +25.5624436,eq=J2000&-c.rs=0.004
1.24	1.28×10^{-14}		I/297/out	NOMAD1==1155-0059400&-c=070.2847000 +25.5625917,eq=J2000&-c.rs=
1.24	1.28×10^{-14}	2.90×10^{-16}	I/317/sample	PPMXL=3103086006484443817&-c=070.285025 +25.562486,eq=J2000&-c.r
1.24	1.28×10^{-14}	2.90×10^{-16}	I/317/sample	PPMXL=3103086006526005598&-c=070.285109 +25.562451,eq=J2000&-c.r
1.24	1.28×10^{-14}	2.90×10^{-16}	I/339/hsoy	-c=070.2849441512 +25.5624735697,eq=J2000&-c.rs=0.004
1.24	1.28×10^{-14}	2.90×10^{-16}	I/339/hsoy	-c=070.2851234416 +25.5624466616,eq=J2000&-c.rs=0.004
1.24	1.28×10^{-14}	2.90×10^{-16}	II/311/wise	WISE==J044108.40+253344.8&-c=070.285030 +25.562467,eq=J2000&-c.
1.24	1.28×10^{-14}	2.90×10^{-16}	II/328/allwise	AllWISE==J044108.40+253344.8&-c=070.2850171 +25.5624449,eq=J200

λ [μm]	$\nu F(\nu)$ [W m^{-2}]	Error [W m^{-2}]	Vizier table	Vizier ID
1.24	1.28×10^{-14}	2.90×10^{-16}	II/360/catalog	-c=070.284961 +25.562434,eq=ICRS&-c.rs=0.004
1.24	1.28×10^{-14}	2.66×10^{-16}	J/ApJ/867/105/refcat2	-c=070.28496070 +25.56243416,eq=ICRS&-c.rs=0.004
1.24	1.28×10^{-14}	2.90×10^{-16}	I/353/gsc242	-c=070.28496069846 +25.56243415687,eq=ICRS&-c.rs=0.004
1.24	1.28×10^{-14}	2.90×10^{-16}	IV/34/epic	ID=247966607&-c=070.285121 +25.562456,eq=J2000&-c.rs=0.004
1.25	1.32×10^{-14}	2.40×10^{-17}	II/319/gcs9	-c=070.285011 +25.562462,eq=J2000&-c.rs=0.004
1.25	1.28×10^{-14}	3.12×10^{-16}	II/246/out	2MASS====04410842+2533448 &-c=070.285121 +25.562456,eq=J2000&-c.r
1.25	1.29×10^{-14}	2.88×10^{-16}	II/246/out	2MASS====04410842+2533448 &-c=070.285121 +25.562456,eq=J2000&-c.r
1.25	1.29×10^{-14}	2.88×10^{-16}	IV/38/tic	-c=070.28512515484 +25.56243094699,eq=J2000&-c.rs=0.004
1.25	1.29×10^{-14}	2.88×10^{-16}	IV/39/tic82	-c=070.28512515484 +25.56243094699,eq=J2000&-c.rs=0.004
1.63	1.97×10^{-14}	5.52×10^{-16}	II/246/out	2MASS====04410842+2533448 &-c=070.285121 +25.562456,eq=J2000&-c.r
1.63	1.99×10^{-14}	3.68×10^{-16}	II/246/out	2MASS====04410842+2533448 &-c=070.285121 +25.562456,eq=J2000&-c.r
1.63	1.99×10^{-14}	3.68×10^{-16}	IV/38/tic	-c=070.28512515484 +25.56243094699,eq=J2000&-c.rs=0.004
1.63	1.99×10^{-14}	3.68×10^{-16}	IV/39/tic82	-c=070.28512515484 +25.56243094699,eq=J2000&-c.rs=0.004
1.65	1.89×10^{-14}	3.64×10^{-16}	II/368/sstsl2	-c=070.2850393 +25.5624436,eq=J2000&-c.rs=0.004
1.65	1.98×10^{-14}		I/297/out	NOMAD1====1155-0059400&-c=070.2847000 +25.5625917,eq=J2000&-c.rs=
1.65	1.98×10^{-14}	5.45×10^{-16}	I/317/sample	PPMXL=3103086006484443817&-c=070.285025 +25.562486,eq=J2000&-c.r
1.65	1.98×10^{-14}	5.45×10^{-16}	I/317/sample	PPMXL=3103086006526005598&-c=070.285109 +25.562451,eq=J2000&-c.r
1.65	1.98×10^{-14}	5.45×10^{-16}	I/339/hsoy	-c=070.2849441512 +25.5624735697,eq=J2000&-c.rs=0.004
1.65	1.98×10^{-14}	5.45×10^{-16}	I/339/hsoy	-c=070.2851234416 +25.5624466616,eq=J2000&-c.rs=0.004
1.65	1.98×10^{-14}	5.45×10^{-16}	I/353/gsc242	-c=070.28496069846 +25.56243415687,eq=ICRS&-c.rs=0.004
1.65	1.98×10^{-14}	5.45×10^{-16}	II/311/wise	WISE====J044108.40+253344.8&-c=070.285030 +25.562467,eq=J2000&-c.
1.65	1.98×10^{-14}	5.45×10^{-16}	II/328/allwise	AllWISE====J044108.40+253344.8&-c=070.2850171 +25.5624449,eq=J200
1.65	1.98×10^{-14}	5.45×10^{-16}	II/360/catalog	-c=070.284961 +25.562434,eq=ICRS&-c.rs=0.004
1.65	1.98×10^{-14}	5.45×10^{-16}	IV/34/epic	ID=247966607&-c=070.285121 +25.562456,eq=J2000&-c.rs=0.004
1.65	1.98×10^{-14}	3.64×10^{-16}	J/ApJ/867/105/refcat2	-c=070.28496070 +25.56243416,eq=ICRS&-c.rs=0.004
2.16	1.44×10^{-14}	2.77×10^{-16}	II/368/sstsl2	-c=070.2850393 +25.5624436,eq=J2000&-c.rs=0.004
2.16	1.48×10^{-14}	2.77×10^{-16}	I/317/sample	PPMXL=3103086006484443817&-c=070.285025 +25.562486,eq=J2000&-c.r
2.16	1.48×10^{-14}	2.77×10^{-16}	I/317/sample	PPMXL=3103086006526005598&-c=070.285109 +25.562451,eq=J2000&-c.r
2.16	1.48×10^{-14}	2.77×10^{-16}	I/353/gsc242	-c=070.28496069846 +25.56243415687,eq=ICRS&-c.rs=0.004
2.16	1.48×10^{-14}	2.77×10^{-16}	II/311/wise	WISE====J044108.40+253344.8&-c=070.285030 +25.562467,eq=J2000&-c.
2.16	1.48×10^{-14}	2.77×10^{-16}	II/328/allwise	AllWISE====J044108.40+253344.8&-c=070.2850171 +25.5624449,eq=J200
2.16	1.48×10^{-14}	2.77×10^{-16}	IV/34/epic	ID=247966607&-c=070.285121 +25.562456,eq=J2000&-c.rs=0.004
2.16	1.48×10^{-14}	2.77×10^{-16}	IV/38/tic	-c=070.28512515484 +25.56243094699,eq=J2000&-c.rs=0.004
2.16	1.48×10^{-14}	2.77×10^{-16}	IV/39/tic82	-c=070.28512515484 +25.56243094699,eq=J2000&-c.rs=0.004
2.19	1.41×10^{-14}	2.74×10^{-16}	II/246/out	2MASS====04410842+2533448 &-c=070.285121 +25.562456,eq=J2000&-c.r
2.19	1.41×10^{-14}	2.74×10^{-16}	II/246/out	2MASS====04410842+2533448 &-c=070.285121 +25.562456,eq=J2000&-c.r
2.20	1.27×10^{-14}	1.36×10^{-17}	II/319/gcs9	-c=070.285011 +25.562462,eq=J2000&-c.rs=0.004
2.20	1.30×10^{-14}	1.36×10^{-17}	II/316/gps6	-c=070.285001 +25.562460,eq=ICRS&-c.rs=0.004
2.20	1.30×10^{-14}	1.36×10^{-17}	II/316/gps6	-c=070.285001 +25.562460,eq=ICRS&-c.rs=0.004
2.20	1.31×10^{-14}	1.36×10^{-17}	II/316/gps6	-c=070.285001 +25.562460,eq=ICRS&-c.rs=0.004
3.35	5.42×10^{-15}	1.16×10^{-16}	II/368/sstsl2	-c=070.2850393 +25.5624436,eq=J2000&-c.rs=0.004
3.35	5.45×10^{-15}	6.26×10^{-17}	II/365/catwise	-c=070.2849803 +25.5624328,eq=ICRS&-c.rs=0.004

λ [nm]	$\nu F(\nu)$ [Wm $^{-2}$]	Error [Wm $^{-2}$]	Vizier table	Vizier ID
3.35	5.47×10^{-15}	1.16×10^{-16}	II/311/wise	WISE====J044108.40+253344.8&-c=070.285030 +25.562467,eq=J2000&-c. -c=070.2849805 +25.5624425,eq=J2000&-c.rs=0.004
3.35	5.49×10^{-15}	8.95×10^{-18}	II/363/unwise	-c=070.28496069846 +25.56243415687,eq=ICRS&-c.rs=0.004
3.35	5.50×10^{-15}	1.16×10^{-16}	I/353/gsc242	AllWISE====J044108.40+253344.8&-c=070.2850171 +25.5624449,eq=J200
3.35	5.50×10^{-15}	1.16×10^{-16}	II/328/allwise	-c=070.28512515484 +25.56243094699,eq=J2000&-c.rs=0.004
3.35	5.50×10^{-15}	1.16×10^{-16}	IV/38/tic	-c=070.28512515484 +25.56243094699,eq=J2000&-c.rs=0.004
3.35	5.50×10^{-15}	1.16×10^{-16}	IV/39/tic82	-c=070.28512515484 +25.56243094699,eq=J2000&-c.rs=0.004 -c=070.2850393 +25.5624436,eq=J2000&-c.rs=0.004
3.55	4.71×10^{-15}	8.44×10^{-18}	II/368/sschl2	-c=070.2850393 +25.5624436,eq=J2000&-c.rs=0.004
4.49	2.53×10^{-15}	6.67×10^{-18}	II/368/sschl2	-c=070.2849805 +25.5624425,eq=J2000&-c.rs=0.004
4.60	2.28×10^{-15}	6.52×10^{-18}	II/363/unwise	-c=070.2850393 +25.5624436,eq=J2000&-c.rs=0.004
4.60	2.35×10^{-15}	5.21×10^{-17}	II/368/sschl2	-c=070.2850393 +25.5624436,eq=J2000&-c.rs=0.004
4.60	2.36×10^{-15}	1.96×10^{-17}	II/365/catwise	-c=070.2849803 +25.5624328,eq=ICRS&-c.rs=0.004
4.60	2.38×10^{-15}	5.21×10^{-17}	II/311/wise	WISE====J044108.40+253344.8&-c=070.285030 +25.562467,eq=J2000&-c. -c=070.28496069846 +25.56243415687,eq=ICRS&-c.rs=0.004
4.60	2.39×10^{-15}	5.21×10^{-17}	I/353/gsc242	AllWISE====J044108.40+253344.8&-c=070.2850171 +25.5624449,eq=J200
4.60	2.39×10^{-15}	5.21×10^{-17}	II/328/allwise	-c=070.28512515484 +25.56243094699,eq=J2000&-c.rs=0.004
4.60	2.39×10^{-15}	5.21×10^{-17}	IV/38/tic	-c=070.28512515484 +25.56243094699,eq=J2000&-c.rs=0.004
4.60	2.39×10^{-15}	5.21×10^{-17}	IV/39/tic82	-c=070.28512515484 +25.56243094699,eq=J2000&-c.rs=0.004 -c=070.2850393 +25.5624436,eq=J2000&-c.rs=0.004
5.73	1.39×10^{-15}	1.05×10^{-17}	II/368/sschl2	-c=070.2850393 +25.5624436,eq=J2000&-c.rs=0.004
7.87	5.71×10^{-16}	7.62×10^{-18}	II/368/sschl2	-c=070.2850393 +25.5624436,eq=J2000&-c.rs=0.004
11.56	1.10×10^{-16}	3.94×10^{-17}	I/353/gsc242	-c=070.28496069846 +25.56243415687,eq=ICRS&-c.rs=0.004
11.56	1.10×10^{-16}	3.94×10^{-17}	II/328/allwise	AllWISE====J044108.40+253344.8&-c=070.2850171 +25.5624449,eq=J200
11.56	1.10×10^{-16}	3.94×10^{-17}	IV/38/tic	-c=070.28512515484 +25.56243094699,eq=J2000&-c.rs=0.004
11.56	1.10×10^{-16}	3.94×10^{-17}	IV/39/tic82	-c=070.28512515484 +25.56243094699,eq=J2000&-c.rs=0.004
11.56	1.17×10^{-16}	4.12×10^{-17}	II/368/sschl2	-c=070.2850393 +25.5624436,eq=J2000&-c.rs=0.004
11.56	3.53×10^{-16}	3.63×10^{-17}	II/311/wise	WISE====J044108.40+253344.8&-c=070.285030 +25.562467,eq=J2000&-c. -c=070.2850393 +25.5624436,eq=J2000&-c.rs=0.004
22.09	3.22×10^{-16}	1.57×10^{-16}	II/311/wise	WISE====J044108.40+253344.8&-c=070.285030 +25.562467,eq=J2000&-c.
22.09	4.61×10^{-16}		II/368/sschl2	-c=070.2850393 +25.5624436,eq=J2000&-c.rs=0.004
22.09	4.68×10^{-16}		I/353/gsc242	-c=070.28496069846 +25.56243415687,eq=ICRS&-c.rs=0.004
22.09	4.68×10^{-16}		II/328/allwise	AllWISE====J044108.40+253344.8&-c=070.2850171 +25.5624449,eq=J200
22.09	4.68×10^{-16}		IV/38/tic	-c=070.28512515484 +25.56243094699,eq=J2000&-c.rs=0.004
22.09	4.68×10^{-16}		IV/39/tic82	-c=070.28512515484 +25.56243094699,eq=J2000&-c.rs=0.004